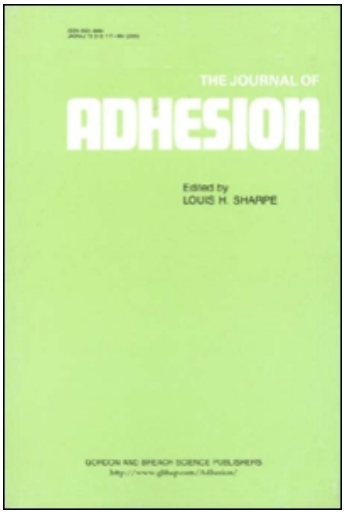

The Journal of Adhesion
Publication details, including instructions for authors and subscription information:
http://www.informaworld.com/smpp/title~content=t713453635

Predicting the Initiation of Thermoset De-Bonding

Douglas B. Adolf[a]; Robert S. Chambers[a]; Brad Hance[a]; Brenton Elisberg[a]
[a] Materials Sciences and Engineering Center, Sandia National Laboratories, Albuquerque, New Mexico, USA

Online publication date: 09 November 2010

To cite this Article Adolf, Douglas B. , Chambers, Robert S. , Hance, Brad and Elisberg, Brenton(2010) 'Predicting the Initiation of Thermoset De-Bonding', The Journal of Adhesion, 86: 11, 1111 — 1131
To link to this Article: DOI: 10.1080/00218464.2010.519259
URL: http://dx.doi.org/10.1080/00218464.2010.519259

The Journal of Adhesion, 86:1111–1131, 2010

ISSN: 0021-8464 print/1545-5823 online
DOI: 10.1080/00218464.2010.519259

Taylor & Francis
Taylor & Francis Group

Predicting the Initiation of Thermoset De-Bonding

Douglas B. Adolf, Robert S. Chambers, Brad Hance, and Brenton Elisberg
Materials Sciences and Engineering Center, Sandia National Laboratories, Albuquerque, New Mexico, USA

Napkin ring adhesion tests over a broad range of experimental conditions suggested a de-bonding mechanism for glassy thermosets associated with "run-away" nonlinear viscoelasticity. Finite element analyses of these tests using a high fidelity, nonlinear constitutive equation were used to identify a single, scalar metric that consistently predicted the initiation of de-bonding, a critical value of the maximum principal strain in the "interphase" zone. In principle, such a de-bonding metric enables evaluation of design margins in practical components.

Keywords: Adhesion; Epoxy; Napkin ring; Prediction; Viscoelasticity

1. INTRODUCTION

Since there have been numerous studies of polymer adhesion, it is important to define the scope and purpose of this study clearly at the outset. First, the investigations focused on the initiation of de-bonding rather than propagation of an existing surface crack. There were no well-defined cracks that one could analyze with fracture mechanics-like approaches. Second, the experimental tests employed a glassy epoxy, so while the results of this study may apply to a wider range of materials, that conjecture is unproven. Third, the interfaces were clean and pristine. De-bonding at mold-released surfaces would invoke mechanisms not probed in these studies, and the surfaces were not aged in humid or solvent-laden atmospheres.

Received 2 March 2010; in final form 9 July 2010.
Sandia is a multiprogram laboratory operated by Sandia Corporation, a Lockheed Martin Company, for the United States Department of Energy's National Nuclear Security Administration under contract DE-AC04-94AL85000.

Address correspondence to Robert S. Chambers, Engineering Sciences Center, Sandia Corporation, Albuquerque, NM 87185-0346, USA. E-mail: rschamb@sandia.gov

Finally, and most importantly, the goal of this investigation centered on developing a quantitative, comprehensive capability to predict de-bonding for arbitrary geometry, temperature, rate, and mode of deformation within a computational finite element stress code. The experiments were used to generate a physically based metric for predicting de-bonding, and detailed finite element simulations of these tests validated its applicability over a variety of test conditions. While the experiments did not cover nearly enough ground to prove universal applicability, a physical de-bonding mechanism was proposed that would enable such broad predictions, and the validation test bed covered both ramped and creep failure tests over a range of temperatures.

If successful, the proposed failure metric could be used within finite element codes to define, for example, critical interfaces in an encapsulated electrical component that may de-bond during thermal cycling due to stresses generated by mismatches in coefficients of thermal expansion. Or one could use it to identify critical impact levels that cause a structural adhesive to de-bond. Both scenarios would examine the "as-designed" component geometry, and more robust designs would fail at lower temperatures during cooling and at higher impact levels in dynamic loading. Therefore, the analyst would use this information to suggest design strategies involving both geometrical and material choices that produce the greatest operational margins. Practically speaking, de-bonding metrics are necessary for margin definition since thermosets appear to de-bond prior to cracking if allowed to do so by the component boundary conditions.

These analyses differ from those employing fracture mechanics on components with identified or pre-defined cracks to determine the stability of the existing cracked configuration. Instead, the proposed analyses would attempt to produce a design that never fails in the first place. Since the vast majority of literature studies either proposes failure metrics but does not validate them with finite element analyses or pursues fracture mechanics approaches inappropriate for initiation of de-bonding, comparison of the current study to existing models in the final section of this paper is rather limited.

2. EXPERIMENTAL

There are a wide variety of experimental adhesion test geometries from which to choose. Since the goal of this program is focused on the development of de-bonding metrics using stresses and strains from computational simulations, it was quite useful for these metrics to be framed directly in terms of stresses or strains rather than fracture mechanics-like quantities that need extensive post processing of the

simulation results. Therefore, a test geometry was needed from which the critical stress and strain at the moment of failure could be extracted cleanly. Typical geometries such as butt tension or lap shear involve complicated stress distributions with rather severe stress risers at the substrate-air-adhesive corner. In fact, fracture mechanics-like approaches have been employed decades ago to analyze tests results in these geometries [1]. One of the few geometries producing a nearly uniform stress state during the test is the napkin ring test pictured in Fig. 1. For a thin annulus relative to the radius, the stress is simply the experimental torque normalized by the area and average radius.

The napkin rings used here were machined from 304 stainless steel. Two surface finishes for the annuli and flat plug were examined: they were polished and blasted with 60 grit red garnet. In a few cases, a gold layer was plated on both polished adherend surfaces. The adherends were bonded together with the annulus as the upper surface, and the bond line (0.5 mm) was set by a steel dowel adjusted with a screw that could be backed off after cure to allow frictionless testing. For annulus and plug constructed from identical material, de-bonding occurred preferentially at the annulus due to the small meniscus formed at the lower, flat plug surface thereby creating a somewhat larger bonding area.

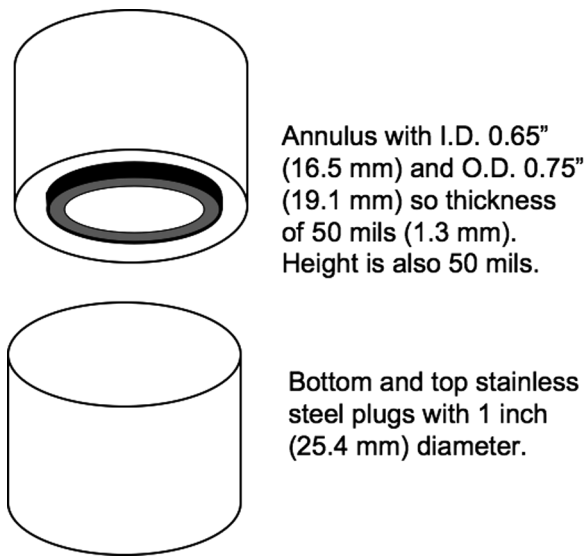

FIGURE 1 The napkin ring test geometry with the dimensions used in this study.

Both controlled displacement torsional ramp (~2% strain/sec) and torsional creep (loaded at 1.7 MPa/sec) tests were performed at various temperatures on a MTS (Eden Prairie, MN, USA) 858 Mini-BionixII servohydraulic axial/torsional test frame. Prior to each test, the bonded napkin ring fixture was heated to 10°C above the adhesive glass transition temperature (Tg), held for 15 minutes to equilibrate in temperature and anneal the epoxy, and then cooled slowly by turning off the oven. The effective epoxy cooling rate was roughly 0.5°C/min from thermocouple measurements on the napkin ring.

Two epoxies were tested. The first system contained diglycidyl ether of bisphenol A (Epon® 828, Hexion, Columbus, OH, USA) cured with diethanol amine (DEA, Fisher Scientific, Waltham, MA, USA) at 12 phr. This system was called "ep1." Its Tg was roughly 70°C when cured for 24 hours at 70°C. The second system contained the same epoxy resin but cured with 12.5 phr of a polyether polyamine (Jeffamine® D230, Huntsman, Salt Lake City, UT, USA) and 12.5 phr of a cycloaliphatic amine (Ancamine® 2049, Air Products, Allentown, PA, USA). Its Tg was roughly 105°C when cured 12 hours at 90°C. This system was called "ep2." Ep2 was tested unfilled and filled with either 43 vol% or 48 vol% of relatively round, monodisperse alumina particles (AA18, Sumitomo Chemical, Tokyo, Japan).

In previous studies [2,3], there appeared to be little dependence of the monotonically loaded, shear stress at failure on resin, filler, or substrate (Figs. 2 and 3). In fact, smooth and rough stainless steel gave similar results. All failures appeared adhesive (for example, Fig. 4).

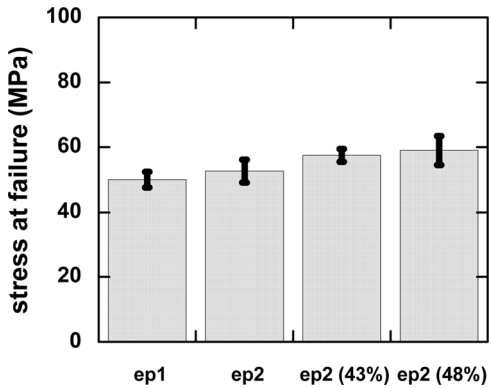

FIGURE 2 The dependence of the shear stress at failure on resin type or filler loading level is not significant.

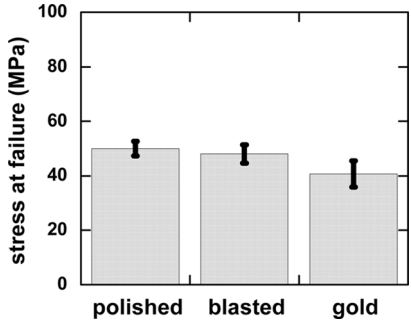

FIGURE 3 The dependence of the shear stress at failure on substrate is not significant. Ep1 was used as the adhesive.

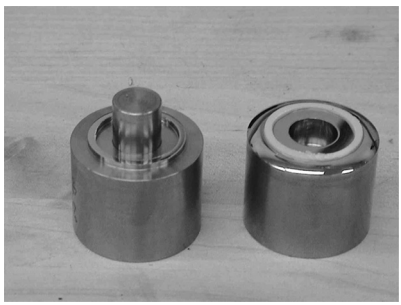

FIGURE 4 Failure in all napkin ring tests appears adhesive. The opaque, alumina filled epoxy is shown here to see the epoxy more clearly.

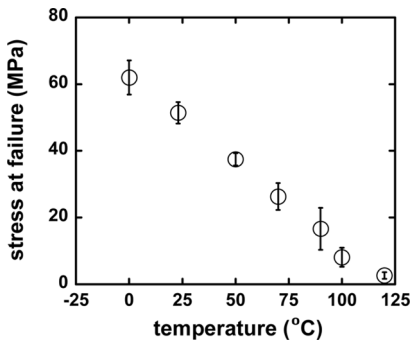

FIGURE 5 The napkin ring shear stress at failure is sensitive to the test temperature.

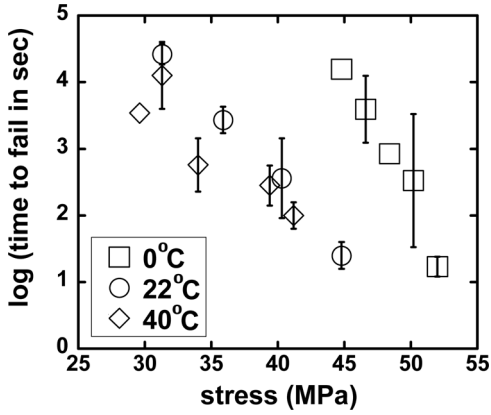

FIGURE 6 The napkin ring time to fail is quite sensitive to both the test temperature and the applied creep load.

The previous studies, however, did indicate significant temperature dependence. Additional results are now presented in Fig. 5 and indicate a linear dependence of the monotonically loaded, shear stress at failure on test temperature. The Tg for the ep1 used in these tests is again roughly 70°C.

The times to fail from torsional creep tests are shown in Fig. 6. Time zero is defined as the end of the ramp loading required to reach the creep stress level. Results from the previous studies showed that the times to fail were very sensitive to the applied stress level at room temperature. Similar results are presented for other temperatures. The sensitivity of the time to fail increases as temperature decreases, and the stresses required to fail at a given time increase as temperature decreases. The latter result is not surprising given the temperature dependence of the critical stress in ramp tests shown in Fig. 5.

3. THEORETICAL

To develop a failure metric from these de-bonding results, the stresses in each test were calculated through a finite element simulation. The tensorial state of stress and strain in each simulation was examined at the moment of experimental failure searching for a single, scalar metric that would be capable of predicting failure in all tests (ramps, holds, temperatures, etc.). All finite element analyses were performed using the ADAGIO code developed at Sandia, although most commercial codes could be used for these relatively simple simulations.

ADAGIO is a Lagrangian, three-dimensional, implicit code for analysis of solids and structures. It employs a multi-level iterative solver to solve problems with large deformations, nonlinear material behavior, and contact. An eight-node uniform strain element was employed in all meshes. The epoxy response was modeled with our previously developed, nonlinear viscoelastic constitutive equation employing a potential energy material "clock." The model was derived [4] from a thermodynamically consistent "rational mechanics" approach that uses the Helmholtz free energy as a potential for defining all thermodynamic quantities. Molecular dynamics studies [5] showed that the mobility of simple chain molecules was a unique function of the system's potential energy, and the rational mechanics framework allowed incorporation of this observation into the constitutive equation. To facilitate acceptance and ease of use, the model was subsequently simplified and called the simplified potential energy clock (SPEC) model [6]. Endless details of the derivation can be found in the references provided, and only the resulting constitutive equation suitable for implementation in ADAGIO or other codes is provided below:

$$\begin{aligned}\underline{\underline{\sigma}} = {} & \frac{\rho}{\rho_{\text{ref}}}\left[K_d(T)\int_0^t ds\ \mathrm{f_v}(\mathrm{t}^*-\mathrm{s}^*)\frac{\mathrm{dI_1}}{\mathrm{ds}} - L_d(T)\int_0^t ds\ \mathrm{f_v}(\mathrm{t}^*-\mathrm{s}^*)\frac{\mathrm{dT}}{\mathrm{ds}}\right]\underline{\underline{\mathrm{I}}} \\ & + \frac{2\rho G_d(T)}{\rho_{\text{ref}}}\int_0^t ds\ \mathrm{f_s}(\mathrm{t}^*-\mathrm{s}^*)\left[\underline{\underline{R}}(t)\cdot\underline{\underline{\mathrm{d}}}_{\mathrm{dev}}(s)\cdot\underline{\underline{R}}(t)^{-1}\right] \\ & + \frac{\rho}{\rho_{\text{ref}}}\left[K_\infty(T)\mathrm{I_1} - L_\infty(T)\{\mathrm{T}-\mathrm{T_{ref}}\}\right]\underline{\underline{\mathrm{I}}} \\ & + \frac{2\rho G_\infty(T)}{\rho_{\text{ref}}}\left[\underline{\underline{R}}\cdot\underline{\underline{\varepsilon}}_{\mathrm{dev}}\cdot\underline{\underline{R}}^{-1}\right]\end{aligned} \tag{1}$$

where $t^*-s^*=\int_s^t \frac{dx}{a(x)}$ and $\log a = -\frac{C_1 N}{C_2''+N}$,

$$\begin{aligned}N = {} & \left[\{T-T_{\text{ref}}\} - \int_0^t ds\ \mathrm{f_v}(\mathrm{t}^*-\mathrm{s}^*)\frac{\mathrm{dT}}{\mathrm{ds}}\right] \\ & + C_3\left[\mathrm{I_1} - \int_0^t ds\ \mathrm{f_v}(\mathrm{t}^*-\mathrm{s}^*)\frac{\mathrm{dI_1}}{\mathrm{ds}}\right] \\ & + C_4\int_0^t\int_0^t ds\,du\ \mathrm{f_s}(\mathrm{t}^*-\mathrm{s}^*,\mathrm{t}^*-\mathrm{u}^*)\underline{\underline{\mathrm{d}}}_{\mathrm{dev}}(s):\underline{\underline{\mathrm{d}}}_{\mathrm{dev}}(u),\end{aligned} \tag{2}$$

where $\underline{\underline{\sigma}}$ is the Cauchy stress, $\underline{\underline{\mathrm{d}}}_{\mathrm{dev}}$ is the deviatoric unrotated rate of deformation tensor, $\underline{\underline{\varepsilon}}$ is its integral with first invariant, $\mathrm{I_1}$, T is temperature, ρ is density (ρ_{ref} is the density at the arbitrary, unstrained

reference state), and $\underline{\underline{R}}$ is the rotational component of the deformation gradient. The required material properties are typical: the decaying and equilibrium bulk and shear moduli (K_d, K_∞, G_d, G_∞), the decaying and equilibrium coefficients of thermal expansion ($L_d = K_d\alpha_d$, $L_\infty = K_\infty\alpha_\infty$), two relaxation spectra corresponding to the volumetric and shear terms (f_v, f_d), and the usual two WLF coefficients (C_1, C_2). Only two new parameters are required that describe (among other phenomena) the pressure dependence of the glass transition and the acceleration of relaxation rates under applied deformations that produces yield (C_3, C_4).

The model was previously parameterized and accurately predicted a wide range of responses seen in glassy polymers [6–8]: temperature dependent yield in compression and tension, change in the apparent glass transition temperature with pressure, a smooth transition between the glassy and rubbery heat capacities and coefficients of thermal expansion, enthalpy relaxation, increase in the yield stress with time (*i.e.*, physical aging), tensile creep at different temperatures and cooling rates, and even coupled effects such as extreme enthalpy relaxation after application of large stresses. Example predictions are shown in Figs. 7–10. In addition, it successfully predicted these responses for several thermosets, a thermoplastic (polycarbonate), and epoxies filled with various particulates past 40 vol% [9]. It has also been extended to predict stresses during thermoset cure by including the extent of reaction as a new dependent variable and tracking the changes in material properties with cure [10].

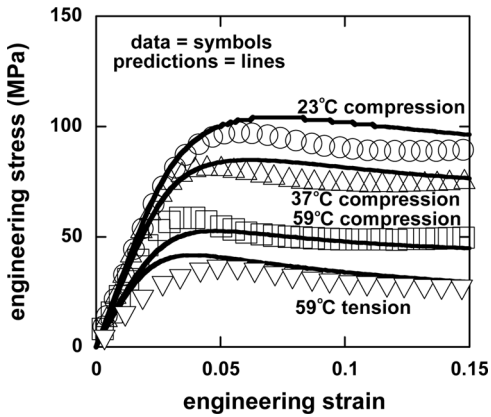

FIGURE 7 Yield of the DEA-cured epoxy at different temperatures.

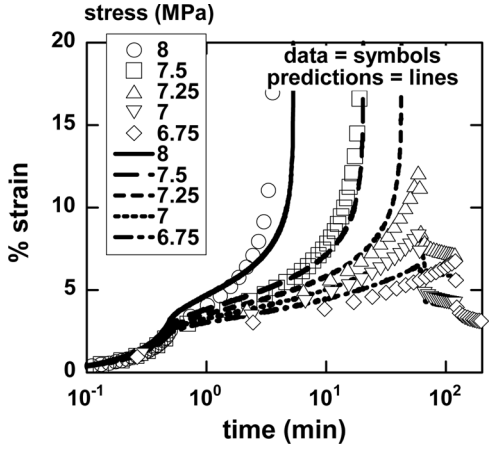

FIGURE 8 Creep of the DEA-cured epoxy at 23°C.

This model is unique in its ability to produce consistently accurate predictions for glassy polymers across such a wide range of tests with a unique, physically based parameter set. Unlike plasticity-based constitutive equations [11], its viscoelastic foundation adheres to the physics underlying the behavior of glassy polymers. As shown later, the epoxy in the ramped de-bonding tests yields, and extensive creep occurs in the creep tests. Models that are created to match, say, only ramped yield data from tension may not predict stresses accurately

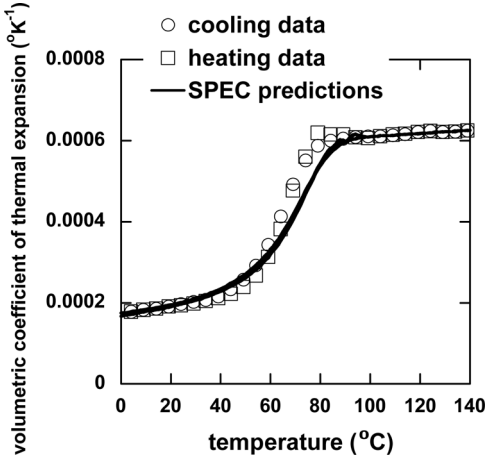

FIGURE 9 Coefficient of thermal expansion of the DEA-cured epoxy.

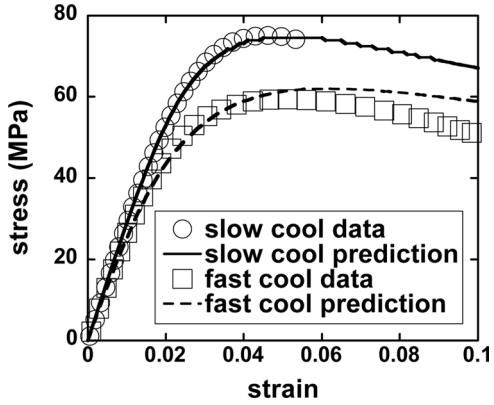

FIGURE 10 Dependence of the compressive stress at 23°C on thermal history.

in shear creep tests at different temperatures. In addition, models that are not physically based may not even predict trends correctly. For example, creep rates for the DEA-cured epoxy were shown [6] to vary by over a factor of 100 for a "slow" *vs.* "fast" cooling rate (Fig. 11). It is imperative to use an extensively validated, high fidelity constitutive equation to believe the large stresses and strains predicted by finite element simulations in complicated, realistic geometries that will be used to predict failure.

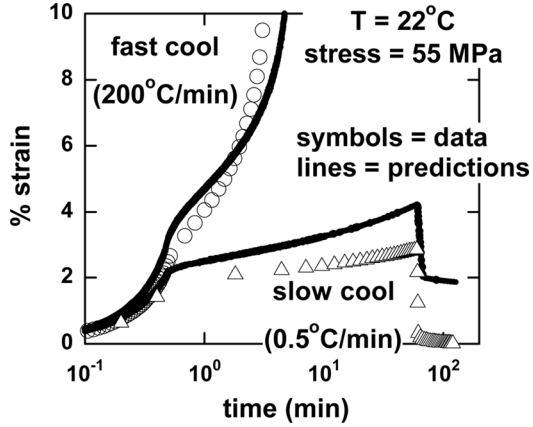

FIGURE 11 Creep rates for the DEA-cured epoxy varied by over a factor of 100 for a slow *vs.* fast cooling rate [6].

4. PREDICTIONS

A section of the finite element mesh for the napkin ring geometry is shown in Fig. 12. Figure 13 shows that the stresses (torque/area/radius) predicted using the SPEC material model for a controlled ramp test in this high fidelity representation of the sample geometry are indistinguishable from a much simpler, single element, shear model. At a more detailed level, the axial (0 to 1, bottom to top in the radial center of the annulus) and radial (0 to 1, inside to outside in the axial center of the annulus) strain distributions were quite uniform (Fig. 14). Note that the shear strains extracted from individual elements in Fig. 14 are components of the tensorial, finite strain tensor and will, therefore, roughly differ from the common engineering strain (shear displacement/specimen thickness) by the factor of two expected in the linear regime. All subsequent simulations used this simplified, single element geometry, but faithfully represented the thermal history of the sample prior to testing. That is, each sample was annealed above Tg and cooled to the test temperature at the experimental rate prior to starting the mechanical loading. Even though the simulated geometry is now trivial (one element), the ADAGIO finite element code (or something similar) is still required to solve the SPEC constitutive equation with its nonlinear hereditary integrals.

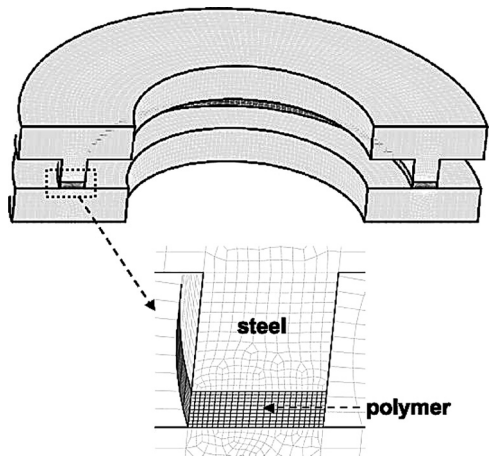

FIGURE 12 A finite element mesh of the napkin ring sample geometry (sliced in half).

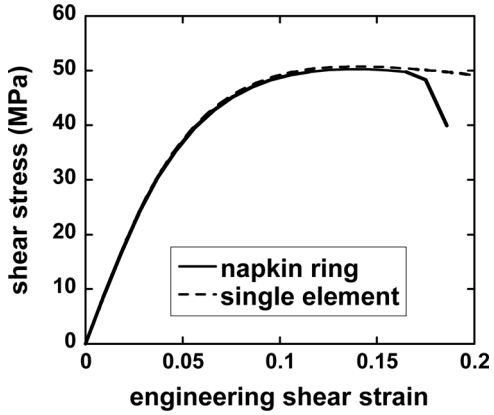

FIGURE 13 Stresses predicted in the napkin ring geometry are indistinguishable from a simple, one element, shear model.

The temperature-dependent ramp and creep experiments described earlier were modeled including details of the thermal equilibration and cooling prior to mechanical testing. In Fig. 15, the measured stresses at failure seemingly tracked the predicted shear yield stresses. In Fig. 16, the predicted creep times at failure were predicted reasonably well by extracting the times at which the predicted strains diverged (see Fig. 8 for examples). Remember from Fig. 11 that creep is extremely sensitive to the exact thermal history so its prediction is much more difficult.

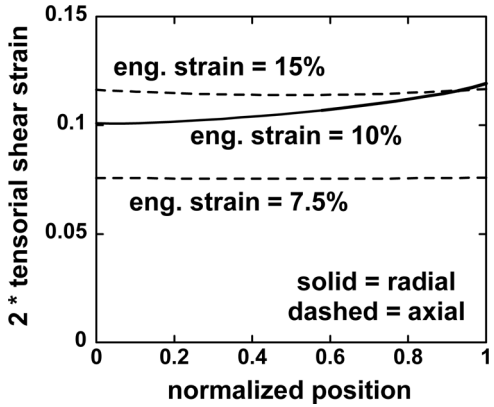

FIGURE 14 The strain distributions are quite uniform in the napkin ring geometry.

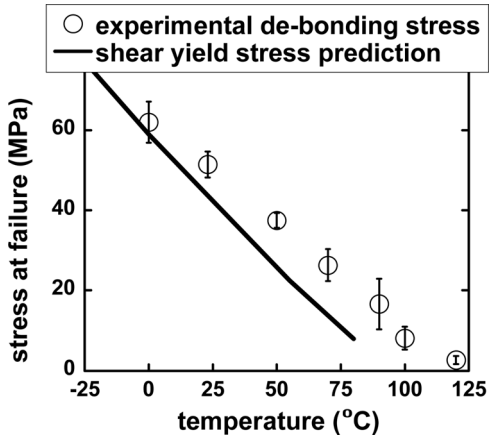

FIGURE 15 The measured stresses at failure correlate with the predicted shear yield stresses.

While the predictive capability is welcome, the mechanism for de-bonding is unclear. All predictions presented in Figs. 15 and 16 arose by examining the bulk response of the epoxy, whereas, every napkin ring failure appeared adhesive by normal interpretation (*i.e.*, "clean" surfaces). Therefore, localization of failure to an interface is not yet predicted. Indeed, our previous studies on cohesive failure [12] showed that the initiation of bulk fracture could be predicted well with the SPEC nonlinear viscoelastic model using a failure metric of a

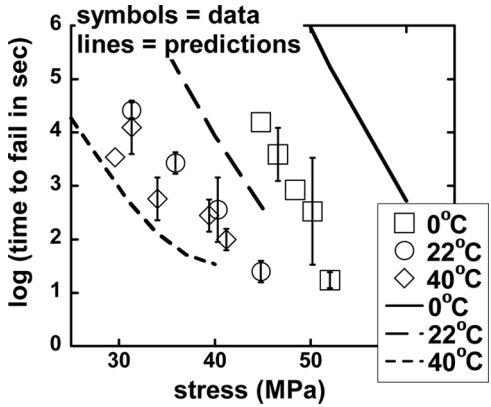

FIGURE 16 The predicted creep times at failure are predicted reasonably well by extracting the times at which the predicted strains diverged.

critical maximum principal strain of roughly 40%. In the following discussion, the ideas used in the cohesive study will be extended to this adhesive investigation.

As a prelude, it is necessary to review extremely quickly and, therefore, incompletely the vast body of work relating to the dynamics of polymers near interfaces begun almost two decades ago [13]. Perhaps a reasonable overview can be gained from the proceedings of the last two "International Workshops on Dynamics in Confinement" [14]. While this research area is quite large, encompassing many types of polymers on different classes of substrates investigated by multiple experimental techniques with, at times, conflicting trends, it is possible that most of the community might agree with the following limited statement. For an annealed, semi-infinite, simple polymer (*e.g.*, an epoxy) adjacent to a relatively non-interacting, inert surface (*e.g.*, stainless steel), the apparent glass transition temperature, Tg, of the polymer near the surface is decreased. A simple but intuitively appealing explanation [15] focuses on the change in density near the interface, which, in turn, affects the packing fraction (or free volume) that controls the polymer dynamics.

If the Tg near the surface is decreased, the polymer in that interphase region will yield prior to the bulk during a ramp-to-fail adhesion test. In the SPEC nonlinear viscoelastic model, yield is a manifestation of increased polymer relaxation rates due to an increase in potential energy during the ramp. The relaxation rates at yield increase to the point that stress decays viscoelastically faster than incremented by the applied ramp producing the characteristic "flattening" of the stress-strain curve. The "weakened" response of the polymer near the surface as it yields first will concentrate the strain in that region as the ramp continues, thereby increasing the potential energy and relaxation rates even faster until the strains are no longer sustainable. A failure criterion based on a relatively large critical maximum principal strain, here in the interphase region, would capture this mechanism. This nonlinear feedback mechanism, or "run-away" nonlinear viscoelasticity, coupled with the decreased Tg near the interface can explain (1) why failure appears adhesive, (2) the severe temperature dependence of the de-bonding stress at failure, (3) the apparent insensitivity to the details of the metallic surface, (4) the relative insensitivity to filler loading levels (*i.e.*, the filler particles cannot occupy the interphase region due to simple space-filling reasons), and (5) why epoxies typically de-bond rather than crack if given the opportunity by the boundary conditions. Note that a polymer near an interacting surface (perhaps a metal with a deposited silane coupling agent) may not exhibit a decreased Tg but, as a result, it may not fail

adhesively but "crack" cohesively. De-bonding in creep is even easier to envision. Again, the relaxation rates of the polymer in the interphase will be faster than in the bulk due to the decreased Tg so the strains under the constant applied load will accumulate faster near the interface leading to "run-away" nonlinear viscoelasticity.

Of course, it may be argued that failure in an interphase regime is not actually adhesive failure. Yet, the failure visually appears "adhesive" as seen in Fig. 4 previously, and the community has known for decades that close inspection of metallic surfaces after de-bonding that "appear" adhesive shows traces of polymer on the substrate (SEM, Auger, etc.) [16]. This remnant polymer does seem to imply a failure "near" but not "at" the metallic surface; however, the mechanism proposed in this study focuses on initiation rather than propagation, and the literature investigations of post-failure interfaces are rigorously limited to inspection of the propagation surface. It would be quite difficult to examine the initiation site since it is vanishingly small. Nevertheless, the proposed mechanism is at least consistent with the literature studies of failure surfaces.

This physical picture was approximately modeled by the simple finite element mesh of a polymer in shear shown in Fig. 17. The bottom face was fixed while the top face was displaced laterally. A periodic displacement boundary condition was assigned to the left and right faces, which allowed the mesh to approximate the napkin ring test. The front and back faces were free. Most importantly, the top and bottom two rows of elements could be assigned a different Tg from the rest of the sample. For illustrative purposes only, the Tg of these interfacial elements was chosen to be either equal to the bulk polymer

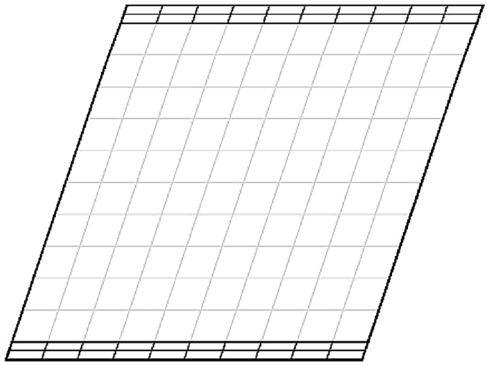

FIGURE 17 Mesh used to investigate the shear response of a polymer with a distinct interfacial Tg.

(modeled as ep1 of Section 2 with Tg $\sim$ 70°C) or 5°C lower (chosen arbitrarily) than the bulk polymer.

Prior to yield, the predicted engineering stress (force/area) – strain (displacement/gap) responses in the single element shear geometry, in simulations using the mesh of Fig. 17 with interfacial Tg equal to the bulk polymer and in simulations using the mesh of Fig. 17 with interfacial Tg 5°C lower than the bulk polymer, were all indistinguishable (curves a, b, and c, respectively, in Fig. 18). The simulation with a distinct interfacial Tg exhibited a precipitous drop in stress when the interfacial elements yielded, which occurred prior to bulk yield given the lower interfacial Tg. This premature yielding of the interfacial elements led to strain intensification in the interfacial elements (Fig. 19) and subsequent run-away nonlinear viscoelasticity. Therefore, this very simple simulation is at least consistent with the proposed mechanism.

The physical picture of run-away nonlinear viscoelasticity could be captured most easily within finite element codes by defining a critical maximum principal strain in the interfacial region similar to the approach used previously to predict cohesive cracking [12]. The exact value of the strain would be relatively unimportant as evidenced by Fig. 8 for creep and Fig. 18 for yield. In both types of tests, strains near the failure event increase rapidly at relatively constant stress so an appropriate strain-based metric would be roughly 15% or greater. A value of 40% predicted cohesive cracking in a wide range of experimental tests where, unlike interfacial failure, the strains could be

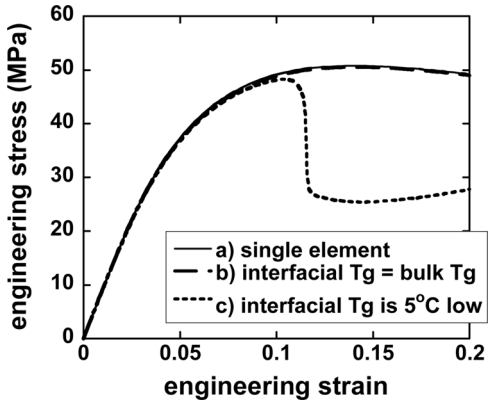

FIGURE 18 The engineering stress-strain responses (a) in the single element shear geometry, (b) in simulations with interfacial Tg equal to the bulk polymer, and (c) in simulations with interfacial Tg 5°C lower than the bulk polymer are indistinguishable prior to yield.

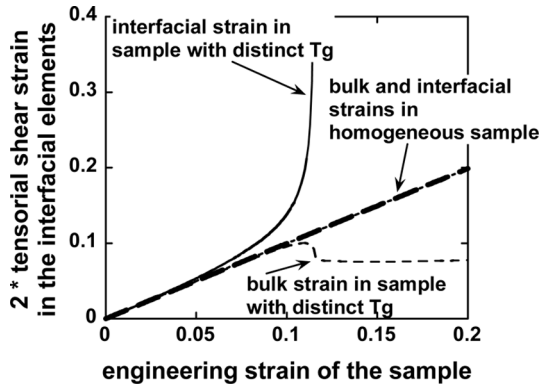

FIGURE 19 The lower Tg of the interfacial elements leads to premature yield and run-away nonlinear viscoelasticity as seen by the dramatic increase in local interfacial (*i.e.*, tensorial element) strain.

calculated accurately (note that engineered stress risers were used in these tests rather than natural cracks to enable accurate geometrical representation). This strain magnitude does not seem unreasonable for these highly cross-linked epoxies with finite network extensibility.

For de-bonding, the physical picture presented above would imply the need to calculate strains near the interface, which would be very difficult due to the small size of the "interphase" region, thereby necessitating inordinately fine meshing. Two engineering approximations might be employed. First, an interfacial element could be developed that incorporated the nonlinear viscoelastic SPEC model enforcing the appropriate boundary for the restricted two-dimensional geometry and assuming an "interphase thickness". De-bonding would again be predicted when the normal or tangential displacement in this interfacial element exceeded a critical value. This approach has the feel of commonly used cohesive zone elements employing traction-separation laws [17], albeit incorporating a physically based material model and failure criterion. However, an easier approach that would at least give engineers an idea of when de-bonding is imminent would simply entail interrogation of the maximum principal strain in an element nearest an interface.

5. COMPARISON WITH PREVIOUS APPROACHES

Few attempts have been made to develop a model capable of predicting the initiation of adhesive de-bonding for arbitrary temperature, mode

of deformation, and stress/strain history. The most complete studies were conducted by ATK Thiokol for development of the multiaxial, temperature, and time-dependent (MATT) failure model [18]. The failure model stands independently from the constitutive framework required to calculate stresses within a component. Assuming this task is complete, the MATT failure model invokes a standard incremental damage model, which in its simplest version is given by

$$\frac{dD}{dt} = \sigma^{\beta} \quad \text{such that } D_c = \int_0^{t_f} ds\sigma^{\beta}, \tag{3}$$

where D is damage, D_c is the critical value of damage indicating failure (a model parameter), t_f is the time at failure, and β is an additional model parameter. Predictions at different temperatures or under different modes of deformation allow D_c and β to depend on temperature and the first and second stress invariants. From the data gathered in their studies, D_c appears relatively constant with temperature while β varies significantly from a value of roughly -24 at 23°C to roughly -10 at 45°C.

In a creep test, Eq. (3) predicts that the time at failure should scale as $\sigma^{-\beta}$. The data and predictions in Fig. 16 are not extensive enough to enable an accurate extraction of the exponent β. However, if gross extrapolations are allowed simply for crude comparison with an existing theory (as shown in Fig. 20), the damage exponents from this study

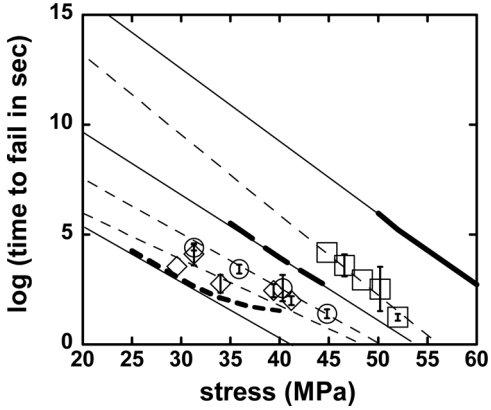

FIGURE 20 The extrapolation procedure for the data (symbols with dashed line extrapolations) and predictions (bold lines with thin, solid line extrapolations) in Fig. 16 that allows comparison with the MATT data.

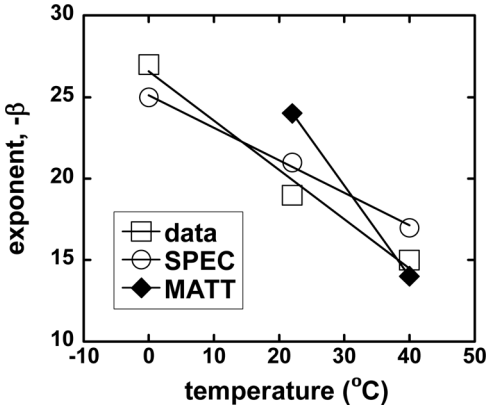

FIGURE 21 The apparent damage exponents from this study (both data and SPEC predictions) and the MATT investigations.

(labeled data and SPEC) and the MATT study are somewhat similar (Fig. 21), especially given the extrapolation inaccuracies and the difference in epoxies used (most likely with distinct Tgs).

The significant difference between the MATT approach and the predictions of the current study perhaps lies in the scope of the studies. The MATT approach bypasses discussion of the constitutive equation and proposes a phenomenological equation for assessing the initiation of de-bonding. In the approach presented in the current study, the stresses were predicted with an accurate and physically based constitutive equation, and the metric for predicting de-bonding was constructed self-consistently from the predicted stresses and strains. While both approaches can be very useful to engineers designing robust components, the current approach offers the possibility of enhanced internal consistency. In addition, from a purely phenomenological perspective, the exponents extracted from the data and used in the MATT model are a bit disconcerting both in their magnitude and dramatic variation with temperature. It is possible that the extremely large values for the exponents ($\sim$25 in some cases) suggests that the functional form of the damage model is not physical, and the variation of this exponent by a factor of over two is most likely the penalty arising from a phenomenological rather than physical framework for predicting de-bonding. The fact that the current, nonlinear viscoelastic approach calculates the local stresses and strains in the sample accurately probably enables a single, constant, scalar metric that predicts failure.

6. CONCLUSIONS

While the napkin ring tests discussed above examined different polymers, fillers, surface textures, substrate composition, temperatures, and strain histories (*e.g.*, ramp *vs.* creep), broader ranges need to be explored in these parameters spaces, as well as investigating different test geometries that incorporate different modes of deformation (*e.g.*, tensile and hydrostatic). Yet, the investigations performed in the current study were extensive enough that it is perhaps surprising for a single constant (a critical maximum principal strain of roughly 25%) to predict de-bonding consistently in all tests. To us, the success of such a simple metric indicates that failure predictions require a high fidelity constitutive equation for the adhesive, which enables calculation of accurate stresses over variations in strain history, temperature, and mode of deformation. While elastic or plastic constitutive laws may be more familiar and, therefore, feel simpler, the price paid for unphysical underpinnings typically appears in failure metrics that are severely dependent on all experimental variables. For example, fracture mechanics approaches typically employ elastic material models, and the resulting critical stress intensity factors need to depend on rate, temperature, mode of deformation, geometry of the stress riser, and surface roughness, to capture even ramp-to-failure data before even considering prediction of creep failure with the additional severe dependence on thermal history. While these dependencies can be ignored theoretically, the experimentalist can be overwhelmed by the tests required to parameterize a single material. In contrast, the experimental path for characterizing the nonlinear viscoelastic SPEC model is only modestly more difficult than required for temperature-dependent thermoelasticity and results in the simplest possible failure metric, a constant.

While the napkin ring experiments and simulations incorporating the SPEC model provided insight into a physical mechanism for failure (*i.e.*, run-away nonlinear viscoelasticity) and identified a simple metric for predicting failure, implementation of this metric into stress analyses of practical components could still be quite difficult. The complex geometries associated with high-value components imply significant computational and meshing obstacles to transparent utilization of the proposed failure metric.

REFERENCES

[1] Ripling, E. J., Mostovoy, S., and Patrick, R. L., *Sixty-Sixth Annual Meeting Papers: Adhesion*, (ASTM, Philadelphia, 1964), pp. 5–19.

[2] Adolf, D. B., Chambers, R. S., Stavig, M. E., and Kawaguchi, S. T., *J. Adhesion* **82**, 63–92 (2006).
[3] Adolf, D. B., Stavig, M. E., Kawaguchi, S., and Chambers, R. S., *J. Adhesion* **83**, 85–104 (2007).
[4] Caruthers, J. M., Adolf, D. B., Chambers, R. S., and Shrikhande, P., *Polymer* **45**, 4577–4597 (2004).
[5] Budzien, J., McCoy, J. D., and Adolf, D. B., *J. Chem. Phys.* **121**, 10291–10298 (2004).
[6] Adolf, D. B., Chambers, R. S., and Neidigk, M. A., *Polymer* **50**, 4257–4269 (2009).
[7] Adolf, D. B., Chambers, R. S., and Caruthers, J. M., *Polymer* **45**, 4599–4621 (2004).
[8] Adolf, D. B., Chambers, R. S., and Flemming, J., *J. Rheology* **51**, 517–540 (2007).
[9] Adolf, D. B. and Chambers, R. S., *J. Polym. Sci B – Polym. Phys.* **43**, 3135–3150 (2005).
[10] Adolf, D. B. and Chambers, R. S., *J. Rheology* **51**, 23–50 (2007).
[11] Hill, R., *The Mathematical Theory of Plasticity*, (Oxford University Press, Oxford, 1998).
[12] Adolf, D. B., Chambers, R. S., Elisberg, B., Stavig, M. E., and Ruff, M., accepted for publication in *J. Appl. Polym. Sci.* DOI: 10.1002/app.32938.
[13] Jackson, C. L. and McKenna, G. B., *J. Non-Cryst. Solids* **131–133**, 221–224 (1991).
[14] McKenna, G. B., *Eur. Phys. J. Special Topics* **141**, 291–301 (2007).
[15] McCoy, J. D. and Curro, J. G., *J. Chem. Phys.* **116**, 9154–9157 (2002).
[16] Bascom, W. D., Timmons, C. O., and Jones, R. L., *J. Mat. Sci.* **10**, 1037–1048 (1975).
[17] Needleman, A., *J. Appl. Mech.* **54**, 525–531 (1987).
[18] Richardson, D. E., McLennan, M. L., Anderson, G. L., Macon, D. J., and Batista-Rodriguez, A., *J. Adhesion* **79**, 157–174 (2003).